Article

Cite This: *Biomacromolecules* 2019, 20, 1362−1374

pubs.acs.org/Biomac

Enhancing the Potency of Antimicrobial Peptides through Molecular Engineering and Self-Assembly

Lucia Lombardi,[†,‡] Yejiao Shi,[‡] Annarita Falanga,[§,∥] Emilia Galdiero,[⊥] Elisabetta de Alteriis,[⊥] Gianluigi Franci,[#] Igor Chourpa,[¶] Helena S. Azevedo,[‡] and Stefania Galdiero*[,†,§]

[†]Department of Pharmacy, School of Medicine, University of Naples Federico II, Via Mezzocannone 16, 80134 Naples, Italy

[‡]School of Engineering and Materials Science, Queen Mary, University of London, Mile End Road, London E1 4NS, United Kingdom

[§]CIRPEB, University of Naples Federico II, Via Mezzocannone 16, 80134 Naples, Italy

[∥]Department of Agricultural Science, University of Naples Federico II, via Università 100, 80055 Naples, Italy

[⊥]Department of Biology, University of Naples Federico II, via Cinthia, 80100 Naples, Italy

[#]Department of Experimental Medicine, University of Campania Luigi Vanvitelli, via Costantinopoli 16, 80138 Naples, Italy

[¶]EA 6295 Nanomédicaments et Nanosondes, Université François-Rabelais de Tours, 31 avenue Monge, 37000 Tours, France

Supporting Information

ABSTRACT: Healthcare-associated infections resulting from bacterial attachment and biofilm formation on medical implants are posing significant challenges in particular with the emergence of bacterial resistance to antibiotics. Here, we report the design, synthesis and characterization of self-assembled nanostructures, which integrate on their surface antibacterial peptides. The antibacterial WMR peptide, which is a modification of the native sequence of the myxinidin, a marine peptide isolated from the epidermal mucus of hagfish, was used considering its enhanced activity against Gram-negative bacteria. WMR was linked to a peptide segment of aliphatic residues (AAAAAAA) containing a lipidic tail ($C_{19}H_{38}O_2$) attached to the ε-amino of a terminal lysine to generate a peptide amphiphile (WMR PA). The self-assembly of the WMR PA alone, or combined with coassembling shorter PAs, was studied using spectroscopy and microscopy techniques. The designed PAs were shown to self-assemble into stable nanofiber structures and these nanoassemblies significantly inhibit biofilm formation and eradicate the already formed biofilms of *Pseudomonas aeruginosa* (Gram-negative bacteria) and *Candida albicans* (pathogenic fungus) when compared to the native WMR peptide. Our results provide insights into the design of peptide based supramolecular assemblies with antibacterial activity, and establish an innovative strategy to develop self-assembled antimicrobial materials for biomedical applications.

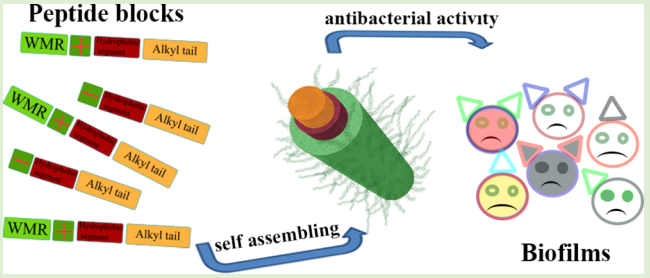

1. INTRODUCTION

The extensive use and misuse of antibiotics for human and animal care have resulted in the development of antibiotic resistant bacteria, which is a major global health problem.[1] The emergence of resistant bacteria calls for the development of new classes of antimicrobial agents to avoid getting back to the preantibiotic era. Severe infections are also frequently associated with biomedical implants (prosthetics, catheters etc.) which have revolutionized medicine but provide an optimal surface for biofilm formation.[2] Furthermore, once developed, biofilms are difficult to treat with standard therapeutic regimens and pose a significant clinical problem with medical devices. Biofilm may be composed of single or multiple species of bacteria and fungi, forming a complex three-dimensional architecture embedded in a self-produced exopolymeric matrix, which renders more difficult the penetration of antibiotics into the matrix and eradicate the pathogenic microorganisms.[3] Managing and preventing biofilm formation is challenging, but can be addressed using materials combined with micro/nanotechnologies.

Recently, great attention has been devoted to peptides with the ability to self-assemble into defined structures and ability to integrate multiple biological functionalities for diverse applications from materials to biomedical sciences.[4,5] Thanks to the proven biocompatibility of peptides, their design flexibility and easy modification by functional groups, self-assembly of peptides offers the possibility to generate highly stable nanostructures combining different functional elements through individually weak noncovalent interactions.[4,5]

Received: December 6, 2018
Revised: February 6, 2019
Published: February 8, 2019

DOI: 10.1021/acs.biomac.8b01740
Biomacromolecules 2019, 20, 1362−1374

In the context of biomedical applications, the development of self-assembling peptides with antibacterial activity has not been widely exploited, although self-assembly is used by nature to fight infections.[6] Most antimicrobial peptides[7] (AMPs) are natural agents produced by both plants and animals, and can self-assemble into fibrillar amyloid-like nanostructures. They interact with the membranes of bacteria and exert their antimicrobial activity by causing membrane damage, being natural weapons for combating microbial infections.[1,8−11] Recently, several studies have been carried out on self-assembling materials to provide model systems for the development of antibacterial agents. In spite of these interests in self-assembling peptides with antibacterial activity, most studies are limited to self-assembling entities to verify their eventual antibacterial activity.[12−14] For example, the antibacterial activity of self-assembled diphenylalanine was recently reported, showing that the diphenylalanine nanoassemblies can inhibit bacterial growth and damage bacterial morphology at a concentration of approximatively 400 μmol/mL.[15] The development of this minimal model of antibacterial materials provides a starting point for engineering more potent self-assembled nanosystems.

In this context, integrating antimicrobial peptides[9] into a self-assembling system offers the opportunity to engineer their antimicrobial activity against a wide range of Gram-positive and Gram-negative bacteria, while reducing hemolysis and allergic responses and potentially the development of resistance.[16] Moreover, particularly attracting is the possibility to combine multiple components, including AMPs and conventional antibiotics, which may assist in reducing both the administration dose of the antibiotic and the development of resistance. The antibacterial properties of AMPs and the possibility to display them on the surface of self-assembled nanostructures may provide a more effective way to enhance the activity of AMPs, establishing an innovative design principle for the development of antibacterial materials. Furthermore, improved biocompatibility is also expected by reducing toxic effects for human cells.[17−19] The multivalent presentation of AMPs on the surface of supramolecular nanostructures provides significant improvements compared to the activity of single soluble peptides. It aids in increasing the stability and half-life of peptides, while augmenting and controlling the local concentration of the active peptides, which enables their enhanced interactions with bacteria.

The spontaneous organization of molecules into ordered aggregates through supramolecular interactions, known as self-assembly, can be achieved by the rational design of individual molecules. Peptide amphiphiles (PAs), molecules containing a hydrocarbon chain attached to a peptide segment, are known to self-assemble into cylindrical nanostructures.[20] PAs offer a versatile self-assembling platform to build supramolecular nanomaterials with demonstrated biomedical applications. Different PA molecules have been designed and exploited by numerous research groups, including the laboratories from Stupp, Tirrell, Deming, Guler, Hamley, and others.[20−29]

As proof of concept, we selected the antimicrobial peptide WMR, which has been previously identified in our lab as a modification of the native sequence of myxinidin, as the key functionality to be displayed in the self-assembled nanomaterials.[30−32] Myxinidin is a marine antimicrobial peptide isolated from the epidermal mucus of hagfish (*Myxine glutinosa* L.).[33,34] It is one of the shortest AMPs discovered so far (12-amino-acid peptide: NH_2-GIHDILKYGKPS-$CONH_2$) with potent antibacterial activity against a wide range of bacteria and yeast pathogens.[33,34] The peptide WMR (13-amino-acid-peptide: NH_2-WGIRRILKYGKRS-$CONH_2$) contains one more tryptophan residue at the N-terminus and a higher number of positively charged amino acids (arginine), compared to the native sequence. These features are essential for its greater antimicrobial activity against *Pseudomonas aeruginosa* as found in previously reported activity and structural studies.[30−32]

This work focuses on the possibility of exploiting the multivalent presentation of AMPs on self-assembled nanostructures to improve antibiofilm activities of two representative species of unresolved medical impact: the Gram-negative bacterium *P. aeruginosa* and the fungus *Candida albicans*.[35,36] The pathogenicity of these species is related to their capability to form structured biofilms on both biotic (mucosae) and abiotic (medical devices) surfaces. In particular, *P. aeruginosa* biofilms are responsible for most lung infections[37] and colonization of medical devices is the leading cause of acute nosocomial pneumonia or sepsis.[38] Furthermore, *C. albicans*, which is the prevalent fungal species of the healthy human microbiota, also forms biofilms, causing localized or even disseminated infections especially in immunocompromised patients.[39] Both *Pseudomonas* and *Candida* biofilms are worldwide diffused and have developed a widespread resistance to classical antibiotics, and were thus chosen in this study as model organisms.

We propose self-assembling antimicrobial peptides based on the WMR sequence to enhance their antibacterial efficacy via multivalent display of the AMP sequence. The antibiofilm activity of self-assembled WMR-based PAs was studied and compared to that of unmodified WMR. Our nanosystem represents a sound strategy to design smart materials, which may also contain a conventional antibiotic and be stimuli responsive (e.g., pH-sensitive), releasing the loaded antibiotic following a change in pH. These nanostructures hold great promise due to their biocompatibility and biodegradability.

2. MATERIALS AND METHODS

2.1. Peptide Synthesis and Purification. *2.1.1. Materials.* Fmoc-protected amino acid derivatives, coupling reagents, and rink amide *p*-methylbenzhydrylamine (MBHA) resin were purchased from Iris Biotech GmbH (Germany). Other chemicals were purchased from Sigma-Aldrich and DelChimica (Italy).

2.1.2. Peptide Synthesis. The PAs listed in Table 1 were synthesized on a rink amide resin. The removal of the Fmoc protecting group on the resin and amino acids was performed with 30% v/v piperidine in DMF for 10 min and the couplings were carried out in the presence of 4 equiv Fmoc-protected amino acid, 4 equiv DIC and 4 equiv oxymapure (first coupling) or 4 equiv amino acid, 4 equiv HATU and 8 equiv DIPEA (second coupling).[40,41] A hydrophobic tail, nonadecanoic acid (C19), was attached to the

Table 1. Sequence and Molecular Weight (Mw) of the Peptides Used in This Study

name	sequence	Mw (g/mol)
WMR	NH_2-WGIRRILKYGKRS-$CONH_2$	1632.88
WMR1PA	NH_2-WGIRRILKYGKRSAAAAAA-$CONH_2$	2059.45
WMR2PA	NH_2-WGIRRILKYGKRSAAAAAAK(C19)-$CONH_2$	2466.79
PA1	NH_2-WKRSAAAAAAK(C19)-$CONH_2$	1410.14
PA2	NH_2-GDDSAAAAAAK(C19)-$CONH_2$	1226.94

DOI: 10.1021/acs.biomac.8b01740
Biomacromolecules 2019, 20, 1362−1374

first lysine at C-terminal end. This lysine was protected with an Mtt group in the side chain, which was removed with about 20 washes with DCM:TFA:TIS 94:1:5 of 2 min each. The free side chain was then used to attach the tail with 2 equiv C19, 2 equiv DIC/oxymapure and 4 equiv DIPEA in DMF/THF 80/20% vol/vol (two overnight couplings). At the end of the synthesis, the peptide was cleaved from the resin with TFA/thioanisole/anisole/water/EDT 82.5/5/5/5/2.5% vol, precipitated in ice-cold diethyl ether and purified in a Phenomenex Jupiter 4 μm Proteo 90 Å 250 × 21.20 mm column with a linear gradient of solvent B (0.1% TFA in acetonitrile) in solvent A (0.1% TFA in water) from 20 to 80% in 25 min with UV detection at 210 nm.

2.2. Preparation of PA Assemblies. For all the experiments, PA assemblies were prepared as follows: PA stock solutions were prepared by dissolving the single peptides in water, then sonicating for 15 min. Different aliquots were taken to prepare aqueous solutions of the single PAs (PA1, PA2) or PA mixtures (PA1+WMR2PA, PA2+WMR2PA) at different concentrations. In the mixtures, the peptide molar ratio was 1:1 and was kept constant for all experiments. Then, the solutions were diluted until the concentration was lower than the critical aggregation concentration and then sonicated for 15 min to break any type of pre-existing aggregates. All the samples were freeze-dried and hydrated with the proper volume of water, buffer or dye, in order to obtain the desired concentrations. All the solutions were left to equilibrate for 1 h.

2.3. Critical Aggregation Concentration (CAC) Determination. The solvatochromic fluorescent probe Nile red is widely used to determine the CAC of self-assembling peptides.[42] Nile red shows a blue shift with decreasing solvent polarity. Since Nile red is poorly soluble in water, there is a large preference to partition aggregates which offer hydrophobic binding sites. Initially, 1 mM methanolic Nile red was prepared. Then, the methanolic Nile red was diluted with water in order to have a final concentration of 500 nM (solution A). A stock peptide solution (0.5 mM) was prepared by dissolving the peptide in water (solution B) and different peptide concentrations were prepared using solution B as a stock and water as diluting solvent. Final solutions were mixed, diluted, sonicated and freeze-dried. The peptide powders were dissolved with the right volume of solution A and allowed to stand in the dark place for 1 h before measurement. Emission spectra for each solution were measured by a Cary Eclipse Varian spectrometer. Spectra were taken between 570 and 700 nm at a slit width of 5 nm, using an excitation wavelength of 550 nm and a 10 nm slit width. The measurements were performed in triplicate. The same experiments were carried out with the peptide mixtures. The data were analyzed by plotting the maximum emission fluorescence corresponding wavelength (y) as a function of peptide concentration (x) and fitting with the sigmoidal Boltzmann equation:[43]

$$y = \frac{A_1 - A_2}{1 + e^{(x - x_0/\Delta x)}} + A_2$$

where the variables A_1 and A_2 correspond to the upper and lower limits of the sigmoid, x_0 is the inflection point of the sigmoid and Δx is the parameter, which characterizes the steepness of the function. The sigmoidal plot allows calculating the CAC value at x_0.

2.4. Secondary Structure Analysis. *2.4.1. Circular Dichroism (CD) Analysis.* CD spectra of PA solutions were recorded from 195 nm to 260 in a Jasco J-810 spectropolarimeter using a 1.0 or 0.1 cm quartz cell at room temperature under a constant flow of nitrogen gas. The 1.0 cm cell was used for samples at concentrations of 2.5, 5 and 10 μM, while for the other concentrations the 0.1 cm cell was more suitable for avoiding the excessive increase of HT voltage. Other experimental settings were as follows: scan speed of 5 nm/min, sensitivity of 50 mdeg, time constant of 16 s, bandwidth of 1 nm. Each spectrum was obtained through averaging three scans, and converting the signal to mean molar ellipticity. CD measurements were carried out for the different peptides alone or in combinations at different concentrations, ionic strengths and pH values.

2.4.2. Raman Spectroscopy Analysis. Aqueous solutions of the peptides PA1, WMR2PA and PA2 alone, or in mixtures PA1+WMR2PA and PA2+WMR2PA, were lyophilized and analyzed under a 10× objective of a LabRam microspectrometer (Horiba SAS, Villeneuve d'Ascq, France). The latter was equipped with a 690 nm laser excitation source (laser power was ca. 27 mW at the sample), an 1800 gr/mm diffraction grating and an air-cooled CCD detector. No sample photodegradation was observed during the measurements. Each spectrum shown is an average of 16 scans of 1 s. The spectral data acquirement and treatment were done using a LabSpec software (Horiba SAS, Villeneuve d'Ascq, France).

2.5. Morphological Characterization. Transmission electron microscopy (TEM) imaging was performed to analyze the morphology of the self-assembled peptide nanostructures. TEM was performed on JEOL 1230 with an accelerating voltage of 80 kV and images were recorded by using a SIS Megaview III wide angle CCD camera. Solutions of peptides and their mixtures were freshly prepared in ultrapure water at a concentration which was higher than their respective CAC. After aging for 24 h, the peptide solutions were loaded onto carbon film coated copper grids with 400 mesh and negatively stained by uranyl acetate. The grids were allowed to dry at room temperature for at least 3 h before collecting the images.

2.6. Surface Charge by ζ-Potential Measurement. The ζ-potential of PA solutions at different concentrations was measured using Zetasizer Nano-ZS (Malvern Instruments, Worcestershire, UK). All measurements were performed at 25 °C, at pH 3, 7 and 10 in triplicate, and 1 h after the sample preparations.

2.7. Proteolytic Stability. Trypsin was added into solutions of WMR and the PA1+WMR2PA or PA2+WMR2PA mixtures at trypsin/peptide molar ratio of 1/500. The concentration of WMR was 100 μM, while the mixture was made using the two peptides at a molar ratio of 1/1 and at a total peptide concentration of 200 μM. All the solutions were prepared in 5 mM Tris-base (pH 8) and incubated at 37 °C. At 1, 3, 4, 24 and 48 h, 100 μL of the sample solutions were taken and injected into the analytical reverse phase high performance liquid chromatography (RP-HPLC, Agilent 1200). The absorbance changes of WMR or WMR2PA were monitored in comparison to the signals of WMR or WMR2PA, which were not treated with trypsin. All the solutions were eluted at 1 mL min^{-1} using a linear gradient of solvent B (0.1% TFA in acetonitrile) in solvent A (0.1% TFA in water) with UV detection at 210 nm. In detail, WMR was eluted using an isocratic hold at 5% B for 3 min then a step to 70% B in 15 min, while the complexes PA1+WMR2PA and PA2+WMR2PA were run with a linear gradient from 20% to 90% B in A in 20 min.

2.8. Antibiofilm Activity. Vero cells, *C. albicans* and *P. aeruginosa* were purchased from ATCC, Rockille, (USA). Cell media were obtained from Gibco, Invitrogen Co. (USA) and Euroclone (Italy). *C. albicans* ATCC 90028 culture grown for 24 h in Triptone Soya Broth medium (TSB) with 1% glucose (Difco) at 37 °C was centrifuged at 5000g (4 °C) for 15 min, washed twice in phosphate buffered saline (PBS, pH 7.0) and resuspended in RPMI-1640 medium at a density of 1 × 10^6 cells/mL. *P. aeruginosa* ATCC 9027 was grown overnight at 37 °C in TBS, washed twice in PBS and resuspended to obtain a suspension equivalent to 1 × 10^5 cells/mL. 100 μL of each culture was dispensed into wells of 96-well polystyrene microtiter plates.

To form biofilms at early stage (24 h biofilms), the plates were incubated at 37 °C for 24 h, whereas to generate biofilms at maturation stage (48 h biofilms), the plates were incubated for 48 h and the medium was renewed after the first 24 h. Amphotericin B and ampicillin were used as positive controls at concentrations ranging from 0.4 to 1.6 mg/mL, and untreated biofilms served as the growth control. Various concentrations of the test molecules were prepared in PBS and added to the wells to prevent cells adherence or to eradicate preformed biofilm.

For biofilm mass quantification, the wells were washed twice with PBS, air-dried for 45 min, and stained with 0.4% crystal violet aqueous solution. Absorbance values were read at 570 nm using a microplate reader (SINERGYTM H4, Biotek Instruments, Winooski, VT, USA BioTek Instruments, Inc.). The effect of test molecules on biofilm eradication was quantified by using the XTT assay that analyses the density of the viable adhered cells measuring the relative metabolic activity using the XTT [2,3-bis (2-methoxy-4-nitro-5-sulfophenyl)-5-

DOI: 10.1021/acs.biomac.8b01740
Biomacromolecules 2019, 20, 1362−1374

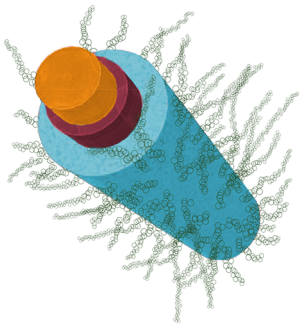

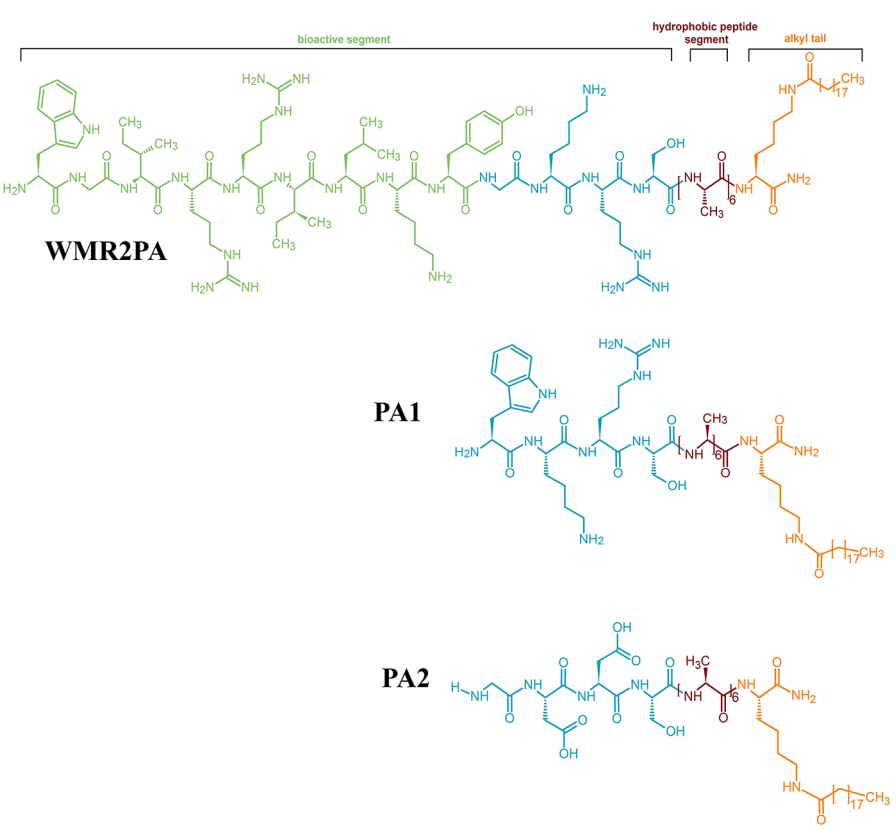

Figure 1. Molecular structure of PAs (WMR2PA, PA1 and PA2) and their suggested self-assembled nanostructure.

(phenylamino)carbonyl)-2H-tetrazolium hydroxide] colorimetric assay Kit (Sigma) following manufacturer's instructions.[44,45]

2.9. Biocompatibility for Mammalian Cells. *2.9.1. Eukaryotic Cell Cytotoxicity.* Vero cells were exposed to increasing concentrations of peptides, and the number of viable cells was determined using the 3-(4,5-dimethylthiazol-2-yl)-2,5-diphenyltetrazolium bromide (MTT) assay that is based on the reduction of the yellowish MTT to the insoluble and dark blue formazan by viable and metabolically active cells.[46] Vero cells were subcultured in 96-well plates at a seeding density of 2×10^4 cells/well and treated with peptides at increasing concentrations 1, 20, 50, 100 and 200 μM for 1 and 24 h. The medium was then gently aspirated, MTT solution (5 mg/mL) was added to each well, and the cells were incubated for further 3 h at 37 °C. The medium with MTT solution was removed, and the formazan crystals were dissolved with dimethyl sulfoxide. The absorption values at 570 nm were measured using a TECAN infinite 200 microplate reader (lifesciences.tecan.com). The viability of Vero cells in each well was presented as a percentage of control cells. All experiments were performed in triplicate and the average with standard deviation was reported. Cell culture without and with 30% DMSO were used as the positive and negative controls, respectively.

2.9.2. Hemolytic Assay. The hemolytic activity of the peptides was determined using fresh human erythrocytes from healthy donors. Twenty-five milliliters of blood was drawn directly into K2-EDTA-coated Vacutainer tubes to prevent coagulation. The blood was then centrifuged at 500*g* for 5 min, and levels of hematocrits were marked. The plasma was gently aspirated and replaced with 150 mM NaCl solution. The solution was then inverted and mixed. The samples were centrifuged at 500*g* for 5 min and resuspended with PBS at pH 7.4. Then, the cells were diluted 1:50 in PBS solution. Peptides were added to the erythrocyte suspension (5% vol/vol), at a final concentration used in the MTT assay with a final volume of 100 μL. The samples were incubated with agitation at 37 °C for 60 min. The release of hemoglobin was monitored by measuring the absorbance (Abs) of the supernatant at 540 nm. The control for zero hemolysis (blank) consisted of erythrocytes suspended in PBS. Detergent (20% Triton X-10) lysed erythrocytes was used as a standard for 100% hemolysis. The percentage of hemolysis was calculated using the following equation:

$$\%\text{haemolysis} = \frac{\text{Abs}_{\text{sample}} - \text{Abs}_{\text{blank}}}{\text{Abs}_{\text{total lysis}} - \text{Abs}_{\text{blank}}} \times 100$$

All experiments were performed in triplicate and the average with standard deviation was reported.

3. RESULTS AND DISCUSSION

3.1. Peptide Design. The molecular design employed in this study is based on a PA design (Figure 1, WMR2PA) and consists of a self-assembling segment composed of aliphatic amino acids (e.g., alanine residues, Figure 1, brown segment) and/or lipid tail (Figure 1, orange segment) attached to an AMP sequence (Figure 1, green segment). The designed WMR2PA is expected to self-assemble into cylindrical nanostructures. In such a system, it would be easy to tune the antibacterial activity by simply changing the AMP sequence on the surface without modifying the self-assembled nanostructures. In addition, to tune the density of the AMP sequence displayed on the surface, we used two different shorter PAs, designed to coassemble with AMP PA (Figure 1, PA1 and PA2). Because antibacterial activity is attained at low concentrations (Minimal Inhibitory Concentrations, MICs, around 10 μM are considered acceptable), it would not be necessary to develop a structure entirely composed of the AMP sequence. In this molecular design, different percentages of the antibacterial sequence can be integrated while the self-assembly is driven by the shorter PAs.

DOI: 10.1021/acs.biomac.8b01740
Biomacromolecules 2019, 20, 1362−1374

The peptide WMR (NH_2-WGIRRILKYGKRS-$CONH_2$) used in this study is a modification of the native sequence of the myxinidin and shows enhanced activity against *Escherichia coli* (MIC 2 μM) and *P. aeruginosa* (MIC 2 μM) bacteria.[30,31] Here, several modifications of WMR were designed.

In the first sequence, we added a six alanine sequence at the C-terminus (WMR1PA: NH_2-WGIRRILKYGKRSAAAAAA-$CONH_2$) (Figure 1, green-turquoise-brown), expecting the aliphatic residues would provide a hydrophobic moiety to drive self-assembly.[47,48] However, this sequence was unable to aggregate at various concentrations and pHs, suggesting that alanines are not sufficient to promote the aggregation. To increase the hydrophobic driving force and favor the aggregation of the peptide, NH_2-WGIRRILKYGKRSAA-AAAA-K(C19)-$CONH_2$ (WMR2PA) was synthesized, which contains a hydrophobic tail on the side chain of the C-terminal lysine residue (C19, composed of 19 carbon atoms) (Figure 1, green-turquoise-brown-orange). This PA was coassembled with a shorter sequence bearing a high tendency to aggregate in order to obtain a self-assembled nanostructure displaying WMR on the surface. We initially designed the short sequence containing the same sequence as the C-terminal part of WMR2PA and bearing a tryptophan at the N-terminus to allow detection by fluorescence spectroscopy (PA1: NH_2-WKRSA-AAAAAK(C19)-$CONH_2$). PA1 was characterized alone and in combination with WMR2PA. To enhance the coassembly, a negative version of PA1 was designed (NH_2-GDDSAAA-AAAK(C19)-$CONH_2$) containing aspartic residues and lacking the tryptophan residue (PA2) which being bulky could hamper the aggregation process. The negatively charged aspartic acid residues are expected to interact electrostatically with the positive residues on WMR2PA (lysine, arginine) and promote cohesion among the peptide molecules. The designed peptide sequences are listed in Table 1 and their chemical structures detailed in Figure 1.

3.2. Peptide Coassembly. *3.2.1. Critical Aggregation Concentration (CAC).* Self-assembling capabilities of single PAs and PA mixtures were analyzed by a fluorescence assay with the fluorophore Nile red. This fluorophore is poorly water-soluble while displaying a large preference to partition in aggregates that offer hydrophobic binding sites and producing a blue shift and hyperchromic effect.

The changes of the emission signal of the Nile red is an indication of the aggregate formation and the concentration at which the changes occur allows the determination of the CAC.

In Figure 2, the wavelength of Nile red maximum fluorescence emission at different concentrations of single peptides is displayed. We used pH 7 (physiological condition) for all peptides and mixtures.

For peptide WMR1PA (Figure 2A), we were unable to observe any blue shift, indicating the inability of this peptide to aggregate under the range of concentrations investigated. The presence of alanines alone was not sufficient to confer the hydrophobic driving force to promote peptide aggregation.

The modified sequence WMR2PA, containing the hydrophobic tail conjugated on the side chain of the C-terminal lysine, was able to aggregate and a CAC value of 5 μM was determined (Figure 2B).

Then, we analyzed the aggregation capabilities of the peptides PA1 and PA2, which were designed to coassemble with WMR2PA. As shown in Figure 2C, peptide PA1 bears a tendency to aggregate and a CAC value of 16 μM was estimated at pH 7. The obtained CAC value for PA2 was 19 μM at pH 7 (Figure 2D).

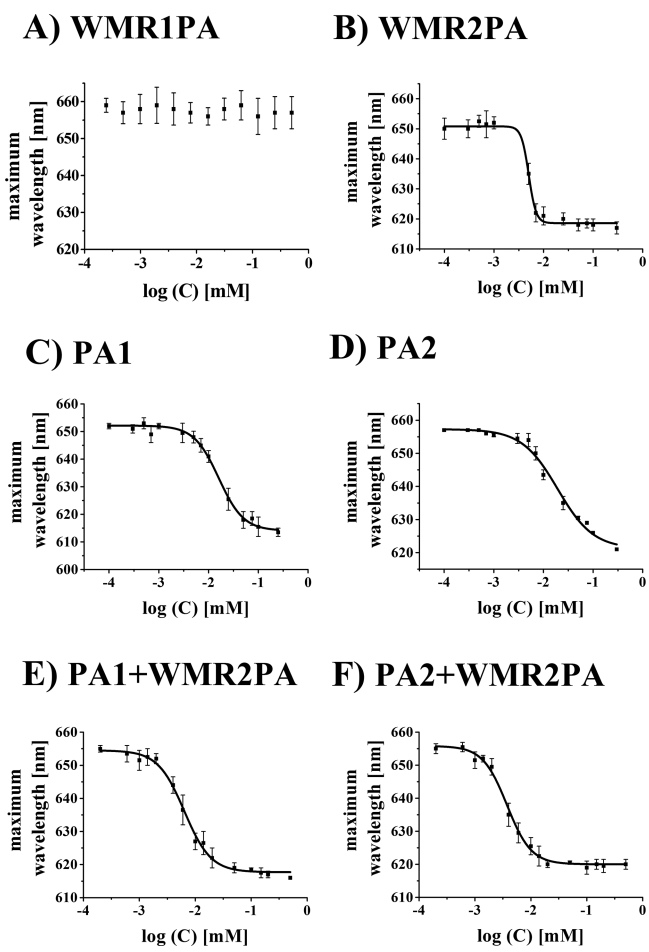

Figure 2. Wavelength corresponding to the maximum fluorescence emission of Nile red was plotted as a function of concentration of the PA: WMR1PA (A), WMR2PA (B), PA1 (C), PA2 (D), and the complex PA1+WMR2PA (E) and PA2+WMR2PA (F) to determine their CAC. The measurements were repeated three times.

From these results, we decided to use WMR2PA as the antimicrobial moiety and both PA1 and PA2 as inducers of the self-assembly process. We have thus focused our analysis on the two complexes PA1+WMR2PA and PA2+WMR2PA (Figure 2E,F).

The mixture PA1+WMR2PA (50% mol/mol) shows a blue shift of Nile red indicating the ability to form aggregates (Figure 2E). The calculated CAC was 6 μM, which is significantly lower than the one obtained for the peptide PA1 alone (16 μM). This is an indication of the ability of PA1 to assist WMR2PA in the aggregation process.

The mixture PA2+WMR2PA (50% mol/mol) also shows the blue shift in the Nile red emission at pH 7 and the calculated CAC is 4 μM; once again, we observe formation of aggregates (Figure 2F).

Table 2 summarized the CAC determined for individual peptides and mixtures. However, fluorescence provides the first glance at the formation of aggregates, but does not give any information about how the peptides interact to self-assemble or the morphology of the nanostructures formed. Additional characterizations were performed to complement these studies.

3.2.2. Secondary Structure. The molecular conformation of the peptides alone or in combination was investigated by far-

DOI: 10.1021/acs.biomac.8b01740
Biomacromolecules 2019, 20, 1362−1374

Table 2. CAC (μM) and ζ-Potential (mV) Values Determined for PAs and Complexes

	WMR1PA	WMR2PA	PA1	PA2	PA1+WMR2PA	PA2+WMR2PA
CAC	–	5	16	19	6	4
ζ-potential		56.5	48.5	−37.9	37	34.8

UV CD spectroscopy, which is an excellent technique for rapid determination of the secondary structure and for studying the formation of peptide assemblies in solution (Figure 3). In fact, self-assembly is often accompanied by changes in secondary structures compared to monomers.

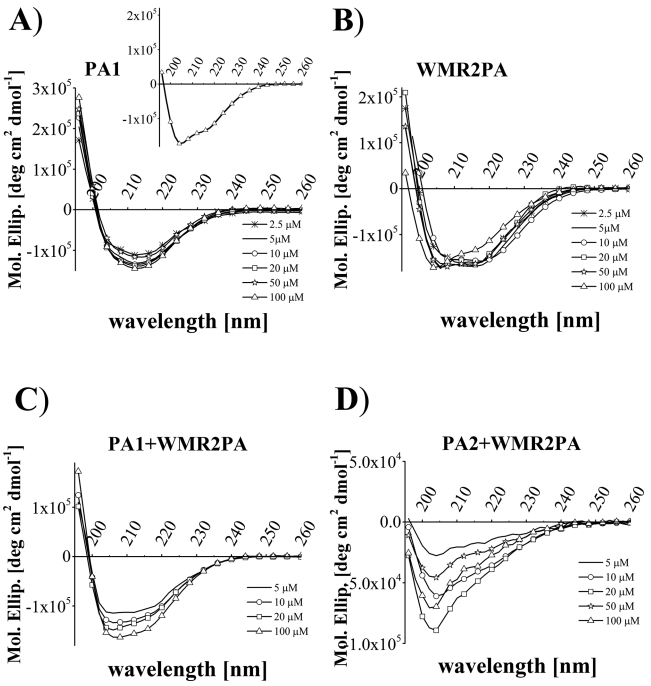

Figure 3. Conformation characterization of PA1 (A) and WMR2PA (B), as well as PA mixtures PA1+WMR2PA (C) and PA2+WMR2PA (D) by CD spectroscopy at different concentrations. The inset of panel A is an enlargement of the spectra for PA1 at 100 μM.

Concentration is a key parameter in controlling the self-assembly of peptides. At very low concentrations, peptides remain as monomers and start to aggregate above the CAC.

The spectrum of the peptide WMR2PA presents a large minimum in the region between 208 and 218 nm. This signal reveals a structure that falls into a noncanonical α-helix or β-sheet conformation, but this pattern may be due to the coexistence of both structures. Nonetheless, the spectrum of the peptide WMR (from which WMR2PA was derived by addition of the moiety necessary for self-assembly) is a typical random coil conformation (data reported in a previous paper);[30,31] although the secondary structure of the WMR2PA monomer may also be different from that of WMR, these spectra were all reported at a concentration close/higher than the CAC, suggesting some sort of aggregations. It is interesting to note that at 100 μM the spectrum obtained assumes features more typical of helical structures; we interpreted this as a proof of aggregation of WMR2PA at higher concentrations supported by the structuring in helical conformation and thus interaction among helices (Figure 3A, inset).

Also for peptide PA1, we observe a trend similar to the one of WMR2PA, which consists in a large band in the region between 208 and 218 nm.

In contrast, the complexes PA1+WMR2PA and PA2+WMR2PA assume a conformation different from the ones adopted by the peptides alone. In the case of the mixture PA1+WMR2PA, the CD spectra show the presence of two minima resembling the typical minima of a helical structure. This characteristic is more evident for the complex PA2+WMR2PA. The CD spectra display the coexistence of α-helix and β-sheet structures with a predominance of the first one.

Raman spectroscopy is well recognized as a structure-specific analytical tool useful in peptide analysis and was used here to characterize the peptides alone (Figure 4A) and their molecular interactions in the mixtures (Figure 4B). The peptides PA1 and WMR2PA have quite similar spectra, with few observable differences (if compared once normalized on the total area in the spectral range shown): the PA1 presents more intense bands at 1295 (Amide III region, α-helix contribution), 1061 and 905 cm^{-1} (C−C stretching modes). In the WMR2PA spectrum, the ratio of the bands at 880/841 cm^{-1} (mainly contributed from Trp W17 and from Tyr Fermi doublets) is decreased and become below 1, possibly due to the Tyr residue being a strong donor of hydrogen bonds. The intensity ratio of the doublet at 757/724 cm^{-1} (mainly contributed from Trp W18) is also decreased for WMR2PA compared to PA1. In contrast to PA1 and WMR2PA, the PA2 is void of aromatic amino acids: as the result, none of the Trp or Tyr bands described above are observed in the spectrum of the PA2 peptide and the band at ca. 1550 cm^{-1} (mainly contributed by Trp) is almost disappeared. In addition, the PA2 has a weaker band at 1436 (CH_2 scissoring). This band is present in all the peptides, and contributed with the W6 mode of Trp when it is present.

The bands at 1236/1217 cm^{-1} (β-sheet)[49] are relatively increased, while the band at 1295 cm^{-1} (α-helix) is higher than for WMR2PA. The C−C stretching bands of the PA2 are also different from those of PA1 and WMR2PA: stronger at 1093 and 905 cm^{-1} and weaker at 1128 cm^{-1}.

We analyzed the spectra obtained for the PA1+WMR2PA and PA2+WMR2PA mixtures and compared them with those obtained from the sum of the spectra of the respective peptides, each normalized and taken at 50%. For the PA1+WMR2PA complex (Figure 4B, curve a), the spectrum shape is very similar to that of the PA1+WMR2PA sum (curve b), the observed changes are weak but concern several bands: increase of the band at 1458 cm^{-1} (CH and/or NH bending) and decrease of the bands at 1668 (antiparallel β-sheet), 1236, 1217, 1093, 905 and 757 cm^{-1} (C−C stretch). For the PA2+WMR2PA, the differences from the sum PA2+WMR2PA are more pronounced and concern even more bands. The decreased bands are the same as for the PA1+WMR2PA complex, except for the band at 757 cm^{-1} that shows a weak increase. In addition, many bands are increased: at 1550 (β-sheet), 1436 (CH_2 scissor), 1295 (α-helix), 1128 (C−C stretch) and 1010 (C−C stretch, W18) cm^{-1}. These changes

DOI: 10.1021/acs.biomac.8b01740
Biomacromolecules 2019, 20, 1362−1374

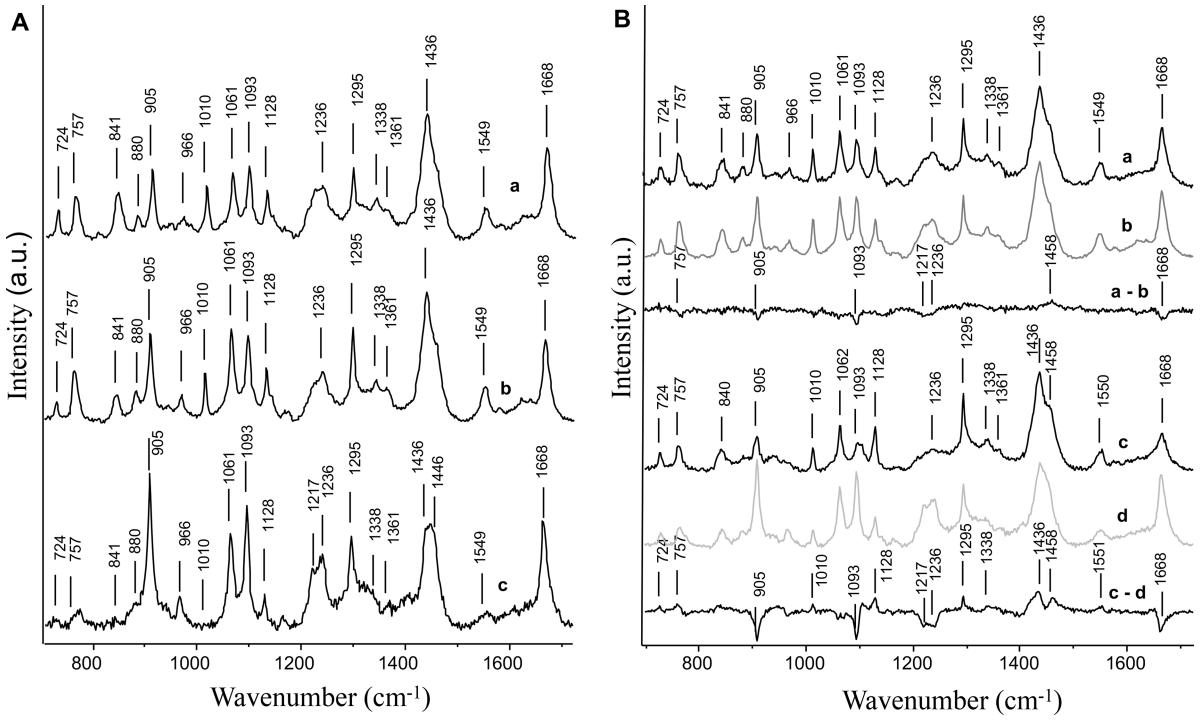

Figure 4. (A) Raman spectra of WMR2PA (a), PA1 (b) and PA2 (c). For better visual comparison, the spectra were normalized on the total intensity with the shown spectral region. (B) Raman spectra of the binary complexes PA1&WMR2PA (a), PA2&WMR2PA (c), the sum of the respective PAs PA1+WMR2PA (b), and PA2+WMR2PA (d) and the respective difference spectra (a-b and c-d).

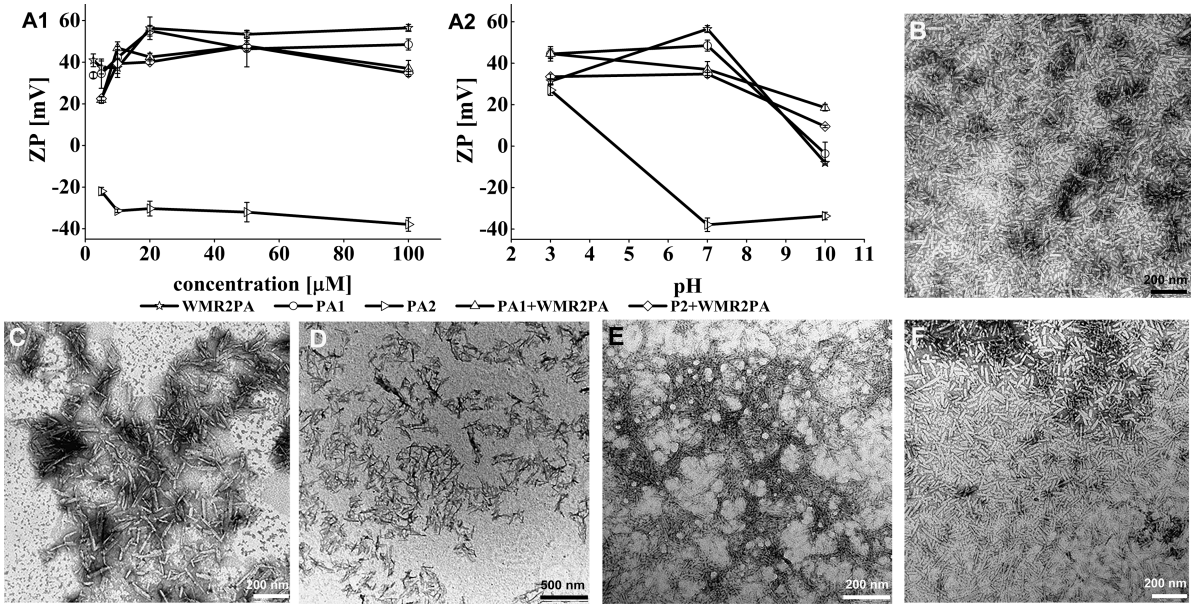

Figure 5. ζ-Potential of the peptides measured at different concentrations and pHs (A). Data are expressed as mean ± standard deviations of three independent experiments. TEM images of nanostructures self-assembled from single PAs WMR2PA (B), PA1 (C) and PA2 (D) and as well as PA mixtures PA1+WMR2PA (E) and PA2+WMR2PA (F).

indicate that peptides underwent a conformational change upon interaction. These changes should be stronger in the PA2+WMR2PA complex, as indicated by the more pronounced spectral changes observed.

The position of the Trp band at 1010 cm^{-1}, known as being sensitive to the strength of van der Waals interactions of the Trp ring with surrounding residues, remains unchanged, thus showing that these interactions were rather weak, in particular within the PA2+WMR2PA complex.

These data indicate that the tryptophan is probably not involved in the self-assembly process and the active moiety is more exposed and free to perform its activity.

3.2.3. Morphology of Self-Assembled Nanostructures. To investigate the morphology of PA assemblies, TEM imaging was carried out. The concentrations of the tested samples were 100 times higher than the CAC values and the pH was 7 for all the collected images. WMR2PA images show the formation of nanostructures with the presence of numerous short fibers; we

DOI: 10.1021/acs.biomac.8b01740
Biomacromolecules 2019, 20, 1362−1374

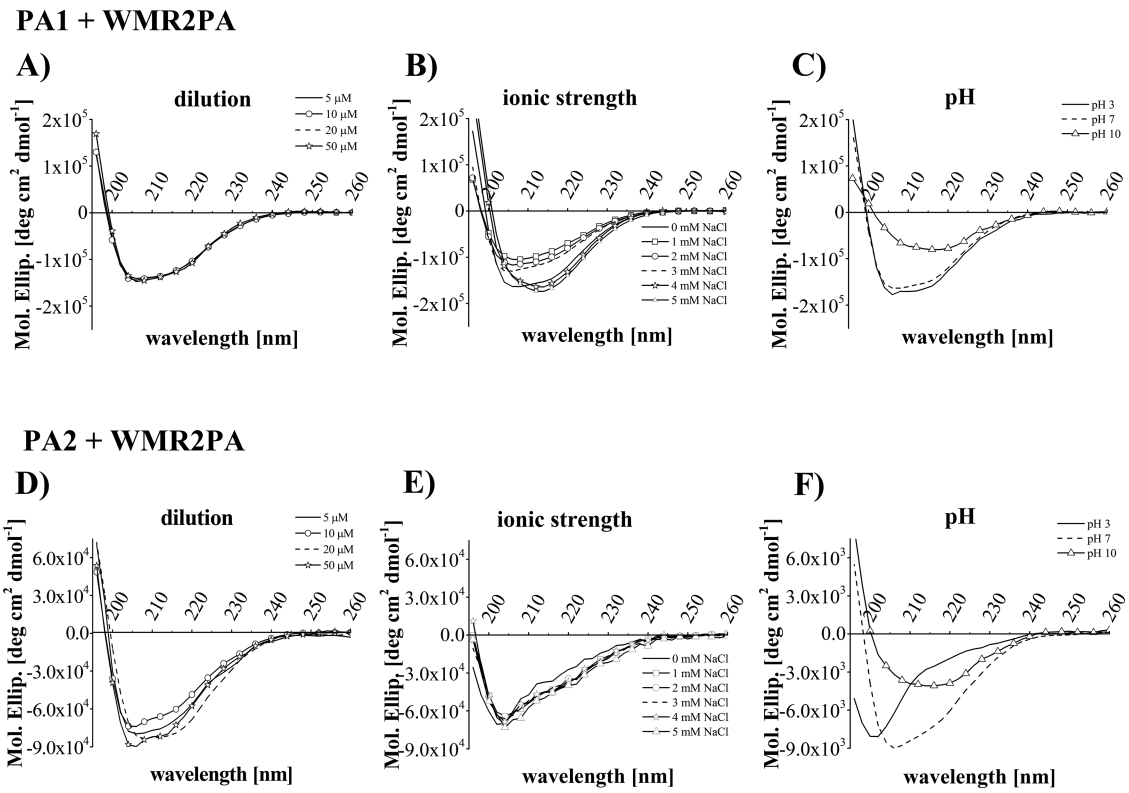

Figure 6. CD spectra of the two complexes PA1+WMR2PA and PA2+WMR2PA upon dilution (A, D) and at different ionic strengths (B, E) and pHs (C, F).

found a CAC of 5 μM for WMR2PA (Figure 2B) indicating that the peptide is able to self-assemble. The design strategy was to reduce the content of the active sequence (the AMP sequence shown in green in Figure 1) and modulate its density on the surface of the self-assembled nanosystem while retaining activity; thus, we were interested in the morphology attained for the complexes. We also analyzed peptides PA1 (CAC 16 μM) and PA2 (CAC 19 μM), which bear respectively a positive and a negative charge, by TEM. For both, TEM shows that aggregation takes place with the formation of short belts for PA1 and short thin fibers for PA2 (Figure 5C,D).

When PA2 is mixed with WMR2PA (Figure 5F), we also observed short fibers very similar to the ones formed by WMR2PA alone (Figure 5B); while, when PA1 is mixed with WMR2PA (Figure 5E), we observe the formation of long fibers. The tryptophan may promote the elongation of the fibers, which are not arranged in a network; rather, they are intertwined in several entanglements. Moreover, at neutral pH the complexes PA1+WMR2PA and PA2+WMR2PA present distinct ζ-potential values (Figure 5A); thus, the difference in fiber length maybe not only due to the presence of tryptophan but also the balance of electrostatic and hydrophobic forces among the molecules.

3.2.4. ζ-Potential. Analysis of the ζ-potential results clearly indicates that both peptides alone and complexes are stable under the conditions tested; the ζ-potential values are typical of monodispersed preparations[50] (Figure 5A1). A positive ζ charge was obtained for the peptides PA1 and WMR2PA, while a negative ζ charge was obtained for PA2, as expected. The TEM images (Figure 5) show that all three peptides are able to assemble in nanostructures at pH 7.

The two complexes both showed positive ζ charges with a lower value for the complex PA2+WMR2PA. The CAC obtained for the complex PA2+WMR2PA is 4 μM (Figure 2F and Table 2) and together with the ζ-potential values indicates the formation of the complex, where the negative charges of PA2 are masked in the self-assembled structures.

Figure 5A2 reports the ζ-potential as a function of pH (pH 3, 7, 10). At pH 10, we observed a ζ-potential between 0 and 20 for all peptides (except PA2), which is indicative of a loss of charge in the self-assembled structures of isolated peptides and of complexes.

3.3. Effect of Concentration, Ionic Strength and pH on Peptide Coassemblies. In order to probe the effect of concentration, ionic strength and pH on the peptide coassembly, circular dichroism spectra were collected at different conditions (Figure 6). Peptide samples were prepared at a total peptide concentration of 100 μM. The solutions were diluted with water and sonicated to break any type of pre-existing interactions; the samples were lyophilized and rehydrated with the correct amount of solvent to achieve the desired concentration. Rehydration was performed only with water to probe the effect of dilution on the pre self-assembled structure, or with NaCl at different concentrations (from 0 to 5 mM NaCl) to probe the effect of the ionic strength and/or aqueous solution at different pHs.

3.3.1. Concentration. To analyze the effect of concentration on the structural stability of the assemblies, a series of diluted solutions of the complexes were prepared and analyzed by CD. We examined the concentration effect on the stability of the self-assembled structures of PA1+WMR2PA and PA2+WMR2-PA (Figure 6A,D). For both complexes, the spectra are completely overlapped even near the CAC value, indicating the absence of any perturbation on the packing of preformed self-assembled nanofibers upon dilution, and also indicating stability of the aggregates. Analyzing the dilution effect is

DOI: 10.1021/acs.biomac.8b01740
Biomacromolecules 2019, 20, 1362−1374

fundamental, in particular for the biological tests, where the self-assembled structures are prepared at concentration well above the CAC, but then diluted.

3.3.2. Ionic Strength. Given the presence of salts in body fluids, we evaluated the effect of ionic strength on the aggregate stability (Figure 6B,E). The complex PA2+WMR2-PA shows the same conformational features of the ones in pure water, indicating stability of the assemblies even in the presence of salts. In contrast, CD spectra of the complex PA1+WMR2PA showed a signal with a predominant β-sheet contribution at 4 and 5 mM NaCl, presumably due to the interactions between the peptides and the salt ions. Increasing concentrations of NaCl could effectively promote the β-sheet conformation when charges of the lysine side chains are screened by Cl^- ions and thus favor the packing of molecules, as also reported in literature.[12] This is evident on the complex PA1+WMR2PA, in which the positive charges of lysines are not balanced by negative charges of the aspartic acid present in the complex PA2+WMR2PA.

3.3.3. pH. The effect of pH on the stability of the self-assembled peptide nanostructures was analyzed by CD at a total peptide concentration of 100 μM (Figure 6C,F). For the PA1+WMR2PA complex, we observed a very similar behavior at pH 3 and 7, while at pH 10 the nanostructures assume a secondary conformation (probably β-sheet), due to the reduced positive net charge, which may favor stronger interactions between peptides.

The pK_a of the lysine side chain is 10.5 and that of the arginine side chain is 12.5. The complex PA1+WMR2PA presents a total of four arginine and three lysine residues. Thus, when the pH is below 10, the two peptides have a total charge of +7 which prevents the flanking sequences from approaching each other and hinders their self-assembly. The spectra at pH 3 and pH 7 are similar and indicative of a helical structure. At pH 10, the majority of the amine groups are unprotonated (neutral, as confirmed by the zeta-potential measurements, Figure 5A) favoring peptide aggregation, as shown by a β-sheet signal in the CD spectrum. The aggregated form may also be attributed to formation of coiled coil structures; in fact, the ratio of ellipticities at 222 and 208 nm, can be used to distinguish between monomeric and oligomeric states of helices.[51] When the ratio $\theta_{222}/\theta_{208}$ equals about 0.8, the peptide is monomeric, and when the ratio exceeds 1.0 it is oligomeric. In our case, we have for PA2+WMR2PA a ratio of 0.2 (pH 3), 0.6 (pH 7) and 1.0 (pH 10), indicating aggregation as a function of pH.

The complex PA2+WMR2PA contains three arginines, two lysines and two aspartic acids, with a total net charge of +3. We observe a different behavior in this complex compared to PA1+WMR2PA, with a different spectrum at each pH (3, 7 and 10). In particular, the peptides started to aggregate at pH 7 with complete aggregation at pH 10.

The data obtained clearly show that the electrostatic interactions play a key role in controlling the nanofiber formation and stability, governing also the disassembly in aqueous solutions.

3.4. Antibiofilm Activity of the Self-Assembled Peptides. To assess the potential of the self-assembled nanostructures to inhibit the formation or to eradicate the preformed biofilms, biofilms of two representative species, the Gram-negative bacterium *P. aeruginosa* and the fungus *C. albicans* were used.

The activity of the sequence WMR against *P. aeruginosa* in planktonic cells was previously reported (MIC 2 μM).[30,31] The activity of WMR against biofilms of both *P. aeruginosa* and *C. albicans* was first tested here. WMR shows less activity against *P. aeruginosa* biofilm compared to planktonic cells. At the lowest concentration tested (12.5 μM), a 20% inhibition was obtained at 24 h of biofilm formation (Figure 7A), while at the

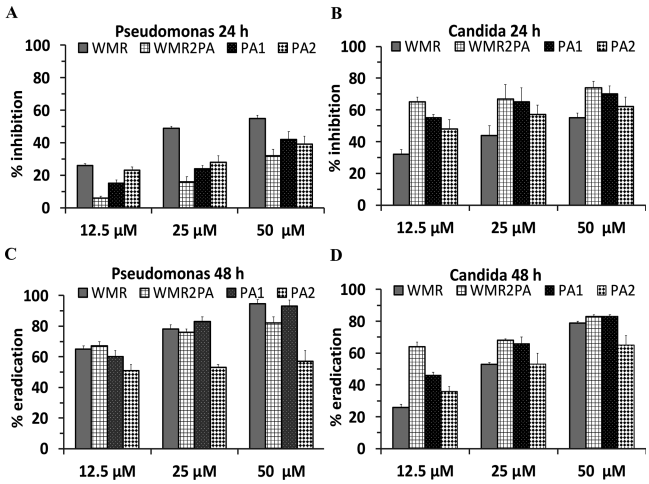

Figure 7. Effect of peptides WMR, WMR2PA, PA1 and PA2 alone on *Pseudomonas* and *Candida* biofilms to evaluate both inhibition (A, B) and eradication (C, D) conditions.

same concentration, complete inhibition of *P. aeruginosa* planktonic cell growth was achieved.[30,31] Interestingly, the activity against a 48 h *P. aeruginosa* biofilm was enhanced indicating that the peptide is able to eradicate the preformed biofilm (Figure 7C). At the same concentration, WMR presents a lower ability to inhibit and eradicate *Candida* biofilms (Figure 7B,D). Nonetheless, both biofilms were impaired at 48 h when using high concentrations (50 μM) of WMR. The next step was to compare the activity of WMR (the native sequence) with that of WMR2PA (which corresponds to WMR modified at the C-terminus with alanines and a hydrophobic tail). The results indicate a loss of activity (concentration-dependent) against *P. aeruginosa* biofilms at 24 h (Figure 7A), whereas an enhanced activity against the *C. albicans* biofilms at 24 h was observed (Figure 7B). Furthermore, we analyzed the effect of P1 and P2, which contain the hydrophobic tail but not the AMP sequence. Surprisingly, we observed recovered activity against *P. aeruginosa* at 24 h and enhanced activity in all other conditions. The analysis of the results show that the hydrophobic tail plays a key role in both inhibition and eradication of *Candida* biofilms, while its role is milder in the inhibition of *Pseudomonas* biofilms, where we observed higher activity for WMR compared to PA sequences. Analysis of the data from the literature on the composition of the outer bacterial (*P. aeruginosa*) and fungal (*C. albicans*) membrane revealed that both are negatively charged but the fungal membrane contains a sterol (ergosterol).[52,53] WMR2PA and PA1 are positively charged while PA2 is negatively charged and they are all aggregated in the condition tested. The charge, while being a key parameter to inhibit *P. aeruginosa* biofilm preventing the initial adhesion of the bacteria (which has a negatively charged surface), may not be the critical parameter in eradication of both biofilms and in the inhibition of *C. albicans*; where a

DOI: 10.1021/acs.biomac.8b01740
Biomacromolecules 2019, 20, 1362−1374

prominent role is played by the hydrophobic tail. PA2 has a net negative charge as the outer membrane of Gram-negative bacteria; thus, we hypothesize that the lipid chain is mainly involved in the interaction with lipids and maybe with the other nonlipidic components of the outer membrane which may determine its mechanism of activity. The role of the C19 in *C. albicans* biofilm may be correlated to the putative interaction with ergosterol. Indeed, the eukaryotic membranes, apart from being zwitterionic, also contain a sterol (cholesterol), but we do not observe toxicity (see next paragraph) at the concentration used. Fungal and eukaryotic membranes differ with respect to sterol identity. Although being structurally similar, their effects on membranes physical parameters are different[52,53] with cholesterol increasing lipid order while maintaining fluidity; the presence of tryptophan residues is also critical because this residue is usually located close to the interface between aqueous solutions and membranes, but due to its bulky nature it is sensitive to sterol identity as reported for other AMPs with antifungal activity and low toxicity for epithelial cells.[54] Thus, we speculated that the C19 tail and the tryptophan are both responsible for the interaction with the ergosterol, which favors their antibacterial and antifungal activity, as well as their low toxicity.

Figure 8 reports the data obtained for the two complexes PA1+WMR2PA and PA2+WMR2PA, in comparison to WMR (the native monomeric sequence). The CACs for the two complexes are 6 and 4 μM, respectively, and the complexes once formed are able to withstand dilution effects; thus, in the condition tested they are self-assembled (Figure 2). Both

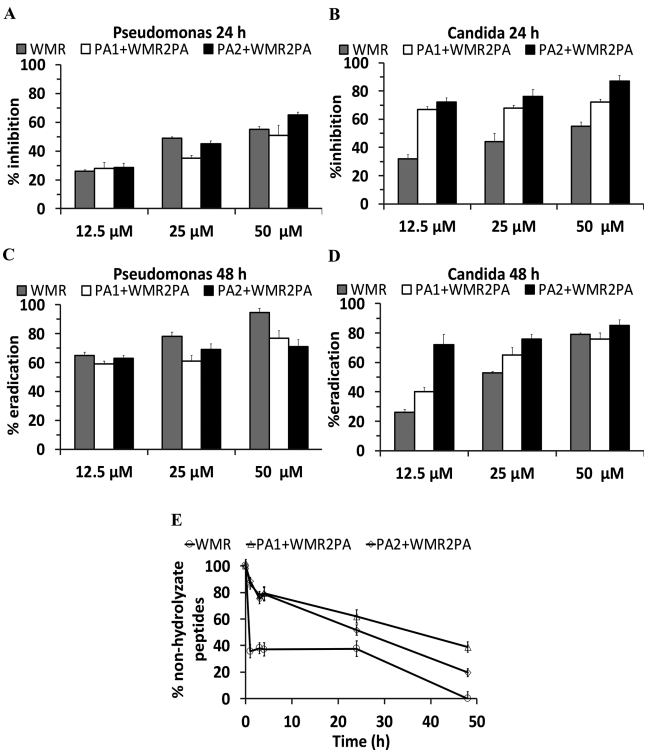

Figure 8. Comparison of PA complexes PA1+WMR2PA and PA2+WMR2PA on *Pseudomonas* and *Candida* biofilms to evaluate both inhibition (A, B) and eradication conditions (C, D). Proteolytic stability of WMR and PA complexes PA1+WMR2PA and PA2+WMR2PA monitored by analytical-HPLC at different incubation times with trypsin (E).

complexes PA1+WMR2PA and PA2+WMR2PA were active against *Candida* biofilms at 24 and 48 h (Figure 8B,D), indicating that they were both effective for biofilm prevention and eradication and they show enhanced activity compared to WMR. On the contrary, we observe comparable activity to WMR for inhibition and eradication of *Pseudomonas* biofilm (Figure 8A,C).

The nanofibers coassembled from the designed peptides not only inhibit the biofilm formation but also eradicate the preformed biofilms, which have been both considered as key processes for applications in antimicrobial therapies. It is likely that prevention of biofilm growth may be related to killing of planktonic bacteria prior to attachment, and for inhibiting adhesion of bacteria, critical initial steps in biofilm formation, which may be attributed not only to the AMP sequence but also to the presence of the hydrophobic tail, which disturbs the formation of the biofilm matrix. Many AMPs are more effective in inhibiting the early phases of biofilm development rather than in eradicating established biofilms.[3] On the contrary, the coassembled nanofibers have shown a strong ability also to eradicate preformed biofilms which may be attributed to their ability to disaggregate the matrix of preformed biofilms, and diffuse into the deep layers of the biofilm killing bacteria inside the biofilm.[3] Overall, these results indicate that a possible mechanism of antibiofilm activity may be related to a "non-classical" mode of action which does not involve only the microbicide effect, but also interference with specific targets of the biofilm lifestyle, such as extracellular matrix production and assembly, and it will be worth to verify whether it is also capable of influencing microorganism cell-to-cell communication and intracellular signaling systems.[3]

The data reported show that both the peptide complexes possess enhanced activity compared to WMR against *Candida* biofilms but a similar activity against *Pseudomonas* biofilm. Although we were unable to enhance activity against *P. aeruginosa* biofilms, we were still able to achieve active complexes and the benefit is represented by their enhanced proteolytic resistance (Figure 8E), which is an added value for therapeutic applications.

3.5. Proteolytic Stability. A significant limitation of peptides as therapeutics is their susceptibility to protease degradation. The proteolytic stability of the self-assembled peptide nanostructures was evaluated by incubation with a common protease enzyme, trypsin, for 48 h and the degradation process was monitored by RP-HPLC. As expected, the native AMP sequence, WMR, was rapidly hydrolyzed by trypsin into two peptide fragments after 1 h (Figures 8E and S1). Chemical modifications of the sequence and formation of self-assembled structures can significantly reduce the enzymatic degradation rate. Both peptide complexes PA1+WMR2PA and PA2+WMR2PA remained stable up to 4 h (Figures 8E and S1). Partial degradations at 24 and 48 h were observed, but a significant part of the active peptide was still present as shown in Figure 8E. After 48 h, we still observe the presence of peak corresponding to the peptide (approximatively 50%). Clearly, the addition of the hydrophobic tail in WMR2PA and the formation of supramolecular assemblies can be used as a viable strategy to improve the protease susceptibilities of antimicrobial peptides.

3.6. Biocompatibility and Selectivity. The selective interaction with bacterial cells, the cytotoxicity toward human cells, as well as the hemolytic activity of the self-assembled peptide nanostructures were evaluated. The results (Figure 9)

DOI: 10.1021/acs.biomac.8b01740
Biomacromolecules 2019, 20, 1362−1374

clearly demonstrate that the self-assembled peptide nanostructures are selective for bacterial cells and are nontoxic for human cells.

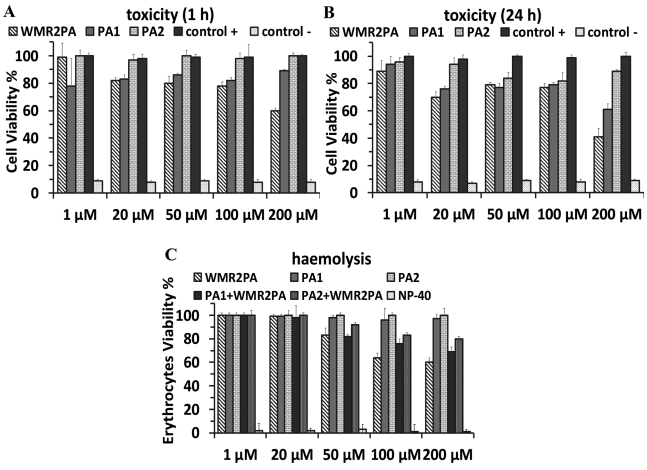

Figure 9. Effect of peptides WMR, PA1, WMR2PA, PA2 and complexes PA1+WMR2PA and PA2+WMR2PA on Vero cells at 1 h (A) and 24 h (B), as well as red blood cells (C) to evaluate their biocompatibility. The detergent NP-40 (octyl phenoxypolyethoxylethanol) was used as positive control in hemolysis studies.

We found low cytotoxicity of the peptide nanostructures on Vero cells even at higher concentration (200 μM) both at 1 and 24 h postexposure (Figure 9A,B). Maximum cell toxicity (60%) was observed for WMR2PA at 200 μM after 24 h. However, WMR2PA is already active against the tested pathogens at lower concentrations, at which the peptide does not show toxicity to mammalian cells. Furthermore, WMR2PA was coassembled with PA1 or PA2, which were clearly nontoxic.

In the evaluation of the hemolytic activity, only WMR2PA shows a partial toxic effect (Figure 9C). This toxicity (less than 50%) was maintained when WMR2PA is associated with the peptides PA1 and PA2. Nevertheless, this toxicity is observed only at higher concentrations, leading to the fact that these peptides present low toxicity and low hemolytic activity at the concentrations used to prepare the nanostructures and for the antibiofilm assays.

4. CONCLUSION

In this study, a proof of concept is provided showing how nanoscale engineering can be exploited to produce supramolecular peptide-based platforms with potent antibacterial activity, improved functionalities, as well as enhanced biocompatibility compared to other antimicrobial agents. This supramolecular peptide-based nanotechnology could serve as an important class of antibacterial compounds for the treatment of intracellular microbial infections.[54]

Novel methods for effective biofilm inhibition and/or eradication are very much needed to prevent infection and consequent rejection of implantable biomaterials. Self-assembly was used here for the multivalent presentation of a known AMP onto defined nanostructures. The presence of AMP sequence on the periphery of the self-assembled nanofibers increases its effective local concentration, compared to soluble peptides, and improves the overall antibacterial activity. The antibiofilm activity is also enhanced under the nanofiber configuration compared to soluble peptides. Moreover, the self-assembled nanostructures can also provide a mean to increase peptide stability and half-life, which is one limitation of peptide therapeutics compared with most other antibiotics. To further improve the antibiofilm properties, the designed nanostructures can be combined with conventional antibiotics. The synergistic combinations have the potential to decrease the effective concentration of the active molecules, as well as to extend their spectrum of action, thereby reducing the spread of resistance, which is often linked to monotherapy regimens. The use of self-assembled nanomaterials described in this work may also allow the integration of other AMPs without compromising the nanostructure for the development of novel antibacterial materials.

■ ASSOCIATED CONTENT

Supporting Information

The Supporting Information is available free of charge on the ACS Publications website at DOI: 10.1021/acs.biomac.8b01740.

Comparison of enzymatic resistance of the antimicrobial peptide WMR alone and in self-assembling fibers (PA1+WMR2PA, PA2+WMR2PA) monitored by HPLC at different time: 1, 3, 4, 24 and 48 h (PDF)

■ AUTHOR INFORMATION

Corresponding Author

*Stefania Galdiero. E-mail: stefania.galdiero@unina.it.

ORCID

Helena S. Azevedo: 0000-0002-5470-1844

Stefania Galdiero: 0000-0002-7849-7024

Funding

Y. Shi and H. S. Azevedo gratefully acknowledge the Seed Award in Science (grant reference number: 210122/Z/18/Z) granted by the Wellcome Trust. S. Galdiero gratefully acknowledges the POR CAMPANIA FESR 2014/2020 “Progetto premio infrastruttura per la medicina di precisione in oncologia”.

Notes

The authors declare no competing financial interest.

■ REFERENCES

(1) Falanga, A.; Galdiero, S. Emerging therapeutic agents on the basis of naturally occurring antimicrobial peptides. In *Amino Acids, Peptides and Proteins*; The Royal Society of Chemistry: 2018; Vol. *42*, pp 190−227.

(2) Riool, M.; de Breij, A.; Drijfhout, J. W.; Nibbering, P. H.; Zaat, S. A. J. Antimicrobial Peptides in Biomedical Device Manufacturing. *Front. Chem.* **2017**, *5*, 63.

(3) Delattin, N.; De Brucker, K.; De Cremer, K.; Cammue, B. P. A.; Thevissen, K. Antimicrobial Peptides as a Strategy to Combat Fungal Biofilms. *Curr. Top. Med. Chem.* **2016**, *17* (5), 604−612.

(4) Mendes, A. C.; Baran, E. T.; Reis, R. L.; Azevedo, H. S. Self-assembly in nature: using the principles of nature to create complex nanobiomaterials. *Wiley Interdiscip. Rev.: Nanomed. Nanobiotechnol.* **2013**, *5* (6), 582−612.

(5) Rad-Malekshahi, M.; Lempsink, L.; Amidi, M.; Hennink, W. E.; Mastrobattista, E. Biomedical Applications of Self-Assembling Peptides. *Bioconjugate Chem.* **2016**, *27* (1), 3−18.

(6) McCloskey, A.; Gilmore, B.; Laverty, G. Evolution of Antimicrobial Peptides to Self-Assembled Peptides for Biomaterial Applications. *Pathogens* **2014**, *3* (4), 791−821.

DOI: 10.1021/acs.biomac.8b01740
Biomacromolecules 2019, 20, 1362−1374

(7) Alves, D.; Olívia Pereira, M. Mini-review: Antimicrobial peptides and enzymes as promising candidates to functionalize biomaterial surfaces. *Biofouling* **2014**, *30* (4), 483−499.
(8) Galdiero, S.; Falanga, A.; Berisio, R.; Grieco, P.; Morelli, G.; Galdiero, M. Antimicrobial peptides as an opportunity against bacterial diseases. *Curr. Med. Chem.* **2015**, *22* (14), 1665−1677.
(9) Scudiero, O.; Nigro, E.; Cantisani, M.; Colavita, I.; Leone, M.; Mercurio, F. A.; Galdiero, M.; Pessi, A.; Daniele, A.; Salvatore, F.; Galdiero, S. Design and activity of a cyclic mini-β-defensin analog: a novel antimicrobial tool. *Int. J. Nanomed.* **2015**, *10*, 6523−6539.
(10) Scudiero, O.; Galdiero, S.; Nigro, E.; Del Vecchio, L.; Di Noto, R.; Cantisani, M.; Colavita, I.; Galdiero, M.; Cassiman, J. J.; Daniele, A.; Pedone, C.; Salvatore, F. Chimeric beta-defensin analogs, including the novel 3NI analog, display salt-resistant antimicrobial activity and lack toxicity in human epithelial cell lines. *Antimicrob. Agents Chemother.* **2013**, *57* (4), 1701−1708.
(11) Scudiero, O.; Galdiero, S.; Cantisani, M.; Di Noto, R.; Vitiello, M.; Galdiero, M.; Naclerio, G.; Cassiman, J. J.; Pedone, C.; Castaldo, G.; Salvatore, F. Novel synthetic, salt-resistant analogs of human beta-defensins 1 and 3 endowed with enhanced antimicrobial activity. *Antimicrob. Agents Chemother.* **2010**, *54* (6), 2312−2322.
(12) Liu, Y.; Yang, Y.; Wang, C.; Zhao, X. Stimuli-responsive self-assembling peptides made from antibacterial peptides. *Nanoscale* **2013**, *5* (14), 6413−6421.
(13) McCloskey, A. P.; Draper, E. R.; Gilmore, B. F.; Laverty, G. Ultrashort self-assembling Fmoc-peptide gelators for anti-infective biomaterial applications. *J. Pept. Sci.* **2017**, *23* (2), 131−140.
(14) Laverty, G.; McCloskey, A. P.; Gilmore, B. F.; Jones, D. S.; Zhou, J.; Xu, B. Ultrashort Cationic Naphthalene-Derived Self-Assembled Peptides as Antimicrobial Nanomaterials. *Biomacromolecules* **2014**, *15* (9), 3429−3439.
(15) Schnaider, L.; Brahmachari, S.; Schmidt, N. W.; Mensa, B.; Shaham-Niv, S.; Bychenko, D.; Adler-Abramovich, L.; Shimon, L. J. W.; Kolusheva, S.; DeGrado, W. F.; Gazit, E. Self-assembling dipeptide antibacterial nanostructures with membrane disrupting activity. *Nat. Commun.* **2017**, *8* (1), 1365−1375.
(16) Beter, M.; Kara, H. K.; Topal, A. E.; Dana, A.; Tekinay, A. B.; Guler, M. O. Multivalent Presentation of Cationic Peptides on Supramolecular Nanofibers for Antimicrobial Activity. *Mol. Pharmaceutics* **2017**, *14* (11), 3660−3668.
(17) Tian, X.; Sun, F.; Zhou, X. R.; Luo, S. Z.; Chen, L. Role of peptide self-assembly in antimicrobial peptides. *J. Pept. Sci.* **2015**, *21* (7), 530−539.
(18) Mitra, R. N.; Shome, A.; Paul, P.; Das, P. K. Antimicrobial activity, biocompatibility and hydrogelation ability of dipeptide-based amphiphiles. *Org. Biomol. Chem.* **2009**, *7* (1), 94−102.
(19) Chen, C.; Hu, J.; Zhang, S.; Zhou, P.; Zhao, X.; Xu, H.; Zhao, X.; Yaseen, M.; Lu, J. R. Molecular mechanisms of antibacterial and antitumor actions of designed surfactant-like peptides. *Biomaterials* **2012**, *33* (2), 592−603.
(20) Hendricks, M. P.; Sato, K.; Palmer, L. C.; Stupp, S. I. Supramolecular Assembly of Peptide Amphiphiles. *Acc. Chem. Res.* **2017**, *50* (10), 2440−2448.
(21) Dooling, L. J.; Tirrell, D. A. Engineering the Dynamic Properties of Protein Networks through Sequence Variation. *ACS Cent. Sci.* **2016**, *2* (11), 812−819.
(22) Welsh, E. R.; Tirrell, D. A. Engineering the extracellular matrix: a novel approach to polymeric biomaterials. I. Control of the physical properties of artificial protein matrices designed to support adhesion of vascular endothelial cells. *Biomacromolecules* **2000**, *1* (1), 23−30.
(23) Zhang, S. Discovery and design of self-assembling peptides. *Interface Focus* **2017**, *7* (6), 20170028.
(24) Vauthey, S.; Santoso, S.; Gong, H.; Watson, N.; Zhang, S. Molecular self-assembly of surfactant-like peptides to form nanotubes and nanovesicles. *Proc. Natl. Acad. Sci. U. S. A.* **2002**, *99* (8), 5355−5360.
(25) Sun, Y.; Wollenberg, A. L.; O'Shea, T. M.; Cui, Y.; Zhou, Z. H.; Sofroniew, M. V.; Deming, T. J. Conformation-Directed Formation of Self-Healing Diblock Copolypeptide Hydrogels via Polyion Complexation. *J. Am. Chem. Soc.* **2017**, *139* (42), 15114−15121.
(26) Nowak, A. P.; Breedveld, V.; Pakstis, L.; Ozbas, B.; Pine, D. J.; Pochan, D.; Deming, T. J. Rapidly recovering hydrogel scaffolds from self-assembling diblock copolypeptide amphiphiles. *Nature* **2002**, *417* (6887), 424−428.
(27) Hamley, I. W.; Dehsorkhi, A.; Castelletto, V.; Furzeland, S.; Atkins, D.; Seitsonen, J.; Ruokolainen, J. Reversible helical unwinding transition of a self-assembling peptide amphiphile. *Soft Matter* **2013**, *9*, 9290−9293.
(28) Hamley, I. W.; Castelletto, V. Self-Assembly of Peptide Bioconjugates: Selected Recent Research Highlights. *Bioconjugate Chem.* **2017**, *28* (3), 731−739.
(29) Ekiz, M. S.; Cinar, G.; Khalily, M. A.; Guler, M. O. Self-assembled peptide nanostructures for functional materials. *Nanotechnology* **2016**, *27* (40), 402002−402039.
(30) Cantisani, M.; Finamore, E.; Mignogna, E.; Falanga, A.; Nicoletti, G. F.; Pedone, C.; Morelli, G.; Leone, M.; Galdiero, M.; Galdiero, S. Structural Insights into and Activity Analysis of the Antimicrobial Peptide Myxinidin. *Antimicrob. Agents Chemother.* **2014**, *58* (9), 5280−5290.
(31) Cantisani, M.; Leone, M.; Mignogna, E.; Kampanaraki, K.; Falanga, A.; Morelli, G.; Galdiero, M.; Galdiero, S. Structure activity relations of myxinidin, an antibacterial peptide derived from Epidermal Mucus of Hagfish. *Antimicrob. Agents Chemother.* **2013**, *57* (11), 5665−5673.
(32) Lombardi, L.; Stellato, M. I.; Oliva, R.; Falanga, A.; Galdiero, M.; Petraccone, L.; D'Errico, G.; De Santis, A.; Galdiero, S.; Del Vecchio, P. Antimicrobial peptides at work: interaction of myxinidin and its mutant WMR with lipid bilayers mimicking the P. aeruginosa and E. coli membranes. *Sci. Rep.* **2017**, *7*, 44425−44440.
(33) Subramanian, S.; Ross, N. W.; Mackinnon, S. L. Comparison of the biochemical composition of normal epidermal mucus and extruded slime of hagfish (Myxine glutinosa L.). *Fish Shellfish Immunol.* **2008**, *25* (5), 625−632.
(34) Subramanian, S.; Ross, N. W.; MacKinnon, S. L. Myxinidin, a novel antimicrobial peptide from the epidermal mucus of hagfish, Myxine glutinosa L. *Mar. Biotechnol.* **2009**, *11* (6), 748−757.
(35) de Alteriis, E.; Maselli, V.; Falanga, A.; Galdiero, S.; Di Lella, F. M.; Gesuele, R.; Guida, M.; Galdiero, E. Efficiency of gold nanoparticles coated with the antimicrobial peptide indolicidin against biofilm formation and development of Candida spp. clinical isolates. *Infect. Drug Resist.* **2018**, *11*, 915−925.
(36) de Alteriis, E.; Lombardi, L.; Falanga, A.; Napolano, M.; Galdiero, S.; Siciliano, A.; Carotenuto, R.; Guida, M.; Galdiero, E. Polymicrobial antibiofilm activity of the membranotropic peptide gH625 and its analogue. *Microb. Pathog.* **2018**, *125*, 189−195.
(37) Rosenthal, V. D.; Al-Abdely, H. M.; El-Kholy, A. A.; AlKhawaja, S. A. A.; Leblebicioglu, H.; Mehta, Y.; Rai, V.; Hung, N. V.; Kanj, S. S.; Salama, M. F.; Salgado-Yepez, E.; Elahi, N.; Morfin Otero, R.; Apisarnthanarak, A.; De Carvalho, B. M.; Ider, B. E.; Fisher, D.; Buenaflor, M. C. S. G.; Petrov, M. M.; Quesada-Mora, A. M.; Zand, F.; Gurskis, V.; Anguseva, T.; Ikram, A.; Aguilar de Moros, D.; Duszynska, W.; Mejia, N.; Horhat, F. G.; Belskiy, V.; Mioljevic, V.; Di Silvestre, G.; Furova, K.; Ramos-Ortiz, G. Y.; Gamar Elanbya, M. O.; Satari, H. I.; Gupta, U.; Dendane, T.; Raka, L.; Guanche-Garcell, H.; Hu, B.; Padgett, D.; Jayatilleke, K.; Ben Jaballah, N.; Apostolopoulou, E.; Prudencio Leon, W. E.; Sepulveda-Chavez, A.; Telechea, H. M.; Trotter, A.; Alvarez-Moreno, C.; Kushner-Davalos, L. International Nosocomial Infection Control Consortium report, data summary of 50 countries for 2010−2015: Device-associated module. *Am. J. Infect. Control* **2016**, *44* (12), 1495−1504.
(38) Percival, S. L.; Suleman, L. Slough and biofilm: removal of barriers to wound healing by desloughing. *J. Wound Care* **2015**, *24* (11), 498−510.
(39) Nobile, V.; Michelotti, A.; Cestone, E.; Caturla, N.; Castillo, J.; Benavente-García, O.; Pérez-Sánchez, A.; Micol, V. Skin photoprotective and antiageing effects of a combination of rosemary

DOI: 10.1021/acs.biomac.8b01740
Biomacromolecules 2019, 20, 1362−1374

(Rosmarinus officinalis) and grapefruit (Citrus paradisi) polyphenols. *Food Nutr. Res.* **2016**, *60*, 31871−31886.
(40) Caporale, A.; Doti, N.; Sandomenico, A.; Ruvo, M. Evaluation of combined use of Oxyma and HATU in aggregating peptide sequences. *J. Pept. Sci.* **2017**, *23* (4), 272−281.
(41) Galdiero, S.; Capasso, D.; Vitiello, M.; D'Isanto, M.; Pedone, C.; Galdiero, M. Role of Surface-Exposed Loops of Haemophilus influenzae Protein P2 in the Mitogen-Activated Protein Kinase Cascade. *Infect. Immun.* **2003**, *71* (5), 2798−2809.
(42) Shi, Y.; Lin, R.; Cui, H.; Azevedo, H. S. Multifunctional Self-Assembling Peptide-Based Nanostructures for Targeted Intracellular Delivery: Design, Physicochemical Characterization, and Biological Assessment. In *Biomaterials for Tissue Engineering. Methods in Molecular Biology*; Chawla, K., Ed.; Humana Press: New York, NY, 2018.
(43) Aguiar, J.; Carpena, P.; Molina-Bolívar, J. A.; Carnero Ruiz, C. On the determination of the critical micelle concentration by the pyrene 1:3 ratio method. *J. Colloid Interface Sci.* **2003**, *258* (1), 116−122.
(44) Stepanovic, S.; Vukovic, D.; Hola, V.; Di Bonaventura, G.; Djukic, S.; Cirkovic, I.; Ruzicka, F. Quantification of biofilm in microtiter plates: overview of testing conditions and practical recommendations for assessment of biofilm production by staphylococci. *APMIS* **2007**, *115* (8), 891−899.
(45) Silva, S.; Pires, P.; Monteiro, D. R.; Negri, M.; Gorup, L. F.; Camargo, E. R.; Barbosa, D. B.; Oliveira, R.; Williams, D. W.; Henriques, M.; Azeredo, J. The effect of silver nanoparticles and nystatin on mixed biofilms of Candida glabrata and Candida albicans on acrylic. *Med. Mycol.* **2013**, *51* (2), 178−184.
(46) Fotakis, G.; Timbrell, J. A. In vitro cytotoxicity assays: Comparison of LDH, neutral red, MTT and protein assay in hepatoma cell lines following exposure to cadmium chloride. *Toxicol. Lett.* **2006**, *160* (2), 171−177.
(47) Castelletto, V.; Barnes, R. H.; Karatzas, K. A.; Edwards-Gayle, C. J. C.; Greco, F.; Hamley, I. W.; Rambo, R.; Seitsonen, J.; Ruokolainen, J. Arginine-Containing Surfactant-Like Peptides: Interaction with Lipid Membranes and Antimicrobial Activity. *Biomacromolecules* **2018**, *19* (7), 2782−2794.
(48) Castelletto, V.; Barnes, R. H.; Karatzas, K. A.; Edwards-Gayle, C. J. C.; Greco, F.; Hamley, I. W.; Seitsonen, J.; Ruokolainen, J. Restructuring of Lipid Membranes by an Arginine-Capped Peptide Bolaamphiphile. *Langmuir* **2019**, *35*, 1302−1311.
(49) Maiti, N. C.; Apetri, M. M.; Zagorski, M. G.; Carey, P. R.; Anderson, V. E. Raman Spectroscopic Characterization of Secondary Structure in Natively Unfolded Proteins: α-Synuclein. *J. Am. Chem. Soc.* **2004**, *126* (8), 2399−2408.
(50) Hiemenz, P. E.; Rajagopalan, R. *Principles of Colloid and Surface Chemistry, Revised and Expanded*; CRC Press: Boca Raton, 1997.
(51) Meng, F.-G.; Zeng, X.; Hong, Y.-K.; Zhou, H.-M. Dissociation and unfolding of GCN4 leucine zipper in the presence of sodium dodecyl sulfate. *Biochimie* **2001**, *83* (10), 953−956.
(52) Ghannoum, M. A.; Janini, G.; Khamis, L.; Radwan, S. S. Dimorphism-associated variations in the lipid composition of Candida albicans. *Microbiology* **1986**, *132* (8), 2367−2375.
(53) Mason, A. J.; Marquette, A.; Bechinger, B. Zwitterionic Phospholipids and Sterols Modulate Antimicrobial Peptide-Induced Membrane Destabilization. *Biophys. J.* **2007**, *93* (12), 4289−4299.
(54) Xu, D.; Jiang, L.; Singh, A.; Dustin, D.; Yang, M.; Liu, L.; Lund, R.; Sellati, T. J.; Dong, H. Designed supramolecular filamentous peptides: balance of nanostructure, cytotoxicity and antimicrobial activity. *Chem. Commun.* **2015**, *51* (7), 1289−1292.

DOI: 10.1021/acs.biomac.8b01740
Biomacromolecules 2019, 20, 1362−1374